Microscopic mechanism of hydrogen intercalation: On the conversion of the buffer layer on SiC to graphene

Ryotaro Sakakibara and Wataru Norimatsu
Department of Materials Science and Engineering, Nagoya University, Nagoya 464–8603, Japan

(Received 2 November 2021; revised 17 June 2022; accepted 17 June 2022; published 29 June 2022)

We report an investigation of the microscopic mechanism of hydrogen penetration and migration in the conversion process of the buffer layer on SiC into quasi-freestanding graphene. By systematically observing the initial stage, we found that hydrogen intercalation initiates locally and simultaneously throughout the terrace, followed by the expansion of the intercalated area, resulting in full graphenization of the buffer layer over the SiC surface. This suggests that hydrogen can penetrate the buffer layer. In addition, we found that the steps on the SiC surface can act as a migration barrier, hindering the migration of hydrogen at the interface across the steps. This series of experimental results provides important insights into the fundamental mechanism of hydrogen intercalation and may help to pave the way toward graphene electronics.

DOI: 10.1103/PhysRevB.105.235442

I. INTRODUCTION

Thermal decomposition of SiC (0001) enables us to grow highly crystalline, single-oriented graphene at the wafer scale directly on the semi-insulating substrate [1,2]. Epitaxial graphene obtained in this way facilitates the development of next-generation electronics such as high-frequency transistors [3,4]. Epitaxial graphene has a so-called buffer layer at the graphene-SiC interface, which is a carbon layer with the $(6\sqrt{3} \times 6\sqrt{3})$ $R30°$ reconstruction on SiC (0001) [5,6]. The buffer layer has a graphenelike honeycomb structure, but about 30% of its carbon atoms are covalently bound to the Si atoms of the SiC (0001) surface, making it electrically insulating. One prominent feature of the buffer layer is that it modifies the electrical properties of the adjacent graphene layer. Due to the remote phonon scattering of the buffer layer, the carrier mobility of graphene decreases with the increasing temperature [7]. Moreover, the buffer layer induces electron doping ($n \sim 10^{13}$ cm^{-2}) to overlying graphene [8]. Since the mobility degradation limits the electronic application of epitaxial graphene, interface modification is essential to realize the true performance of graphene.

Among many methods for interface modification such as nitridation [9] and rapid cooling [10], intercalation of foreign elements is the most popular technique to remove the buffer layer and obtain quasi-freestanding monolayer graphene (QFMLG) on the SiC substrate. Although a wide variety of elements (e.g., H [11], Li [12], O [13], Ga [14], and Au [15]) has been intercalated so far, hydrogen is thought to be the best candidate to obtain QFMLG with high quality. In hydrogen intercalation, the buffer layer sample is annealed in a hydrogen gas atmosphere to terminate Si atoms at the buffer layer/SiC interface with H atoms, thereby decoupling the buffer layer from the substrate to form QFMLG. As a result of the hydrogen intercalation, the carrier mobility of QFMLG shows a weak temperature dependence, since there is no buffer layer at the interface [16]. QFMLG obtained in this way is very flat and homogeneous over the substrate surface and has little graphene-substrate interaction [17]. Furthermore, since H has the smallest atomic radius, the damage to the graphene lattice caused during the intercalation process is smaller than that of all other atomic species. Therefore, hydrogen intercalation is regarded as the most reliable approach for graphene electronics.

However, in practice, it is difficult to terminate all Si atoms at the interface with H atoms, giving rise to H deficiencies [18–20]. Such H deficiencies act as scattering centers, degrading the carrier mobility of QFMLG. For the termination of all Si atoms, a detailed understanding of the mechanism of hydrogen intercalation is necessary. However, despite the fact that the technique has been widely demonstrated [11,16–25], its microscopic mechanism is still not clarified sufficiently. Regarding deintercalation (i.e., desorption of hydrogen from the QFMLG/SiC interface), its mechanism on where hydrogen is desorbed from has been discussed, based on experiments [18,26,27]. On the other hand, the mechanism of (original) hydrogen intercalation is not as clear. In particular, it is not evident where hydrogen actually enters the buffer layer/SiC interface and how intercalation proceeds, since it is difficult for both H_2 molecule and H atom to penetrate the hexagonal lattice of the buffer layer according to theoretical calculations [28,29]. Moreover, it has been difficult to capture the initial stage of hydrogen intercalation experimentally, because the process occurs in a short time after the start of annealing. Here, we show an approach to observe the initial stage of hydrogen intercalation by quickly raising or lowering the temperature. To make this approach more effective, we also performed hydrogen intercalation in a high-pressure (5.5-atm) hydrogen gas atmosphere. Based on experimental results obtained by these techniques, we will discuss the microscopic mechanism of hydrogen intercalation, especially the hydrogen penetration

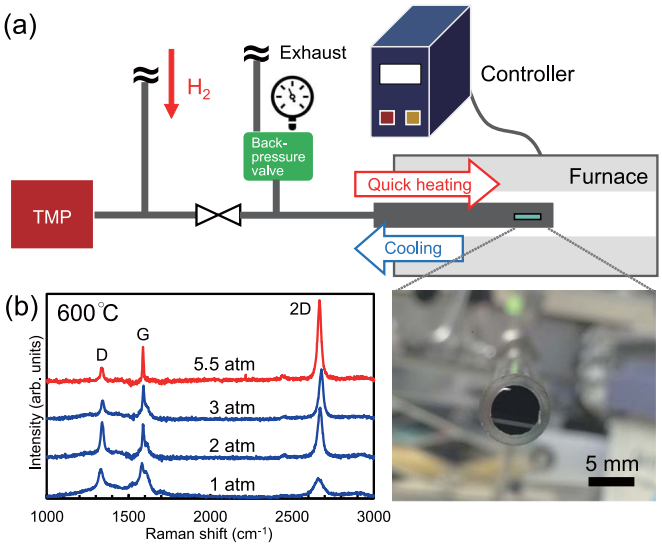

FIG. 1. (a) Schematic illustration of the experimental setup implemented in this study. The photograph below shows the cut plane of the SUS316L tube with a sample substrate inside. (b) Raman spectra of the samples annealed under different pressures of hydrogen gas at 600 °C for 40 min.

into the buffer layer and the hydrogen migration at the interface.

II. EXPERIMENT PROCEDURE

We prepared the homogeneous buffer layer sample by the conventional thermal decomposition method [2,30]. A nominally on-axis, *n*-doped 4H-SiC (0001) wafer was cut into 5×5-mm^2 pieces after chemical mechanical polishing. Prior to the growth, the substrates were cleaned by ultrasonication in ethanol and acetone, followed by a treatment in 10 wt. % of hydrofluoric acid to remove the surface oxide layers. Buffer layer growth was carried out by annealing the substrate at 1500 °C for 3 min under an atmospheric pressure of Ar (99.9999%) with a flow rate of 0.1 slm [10,31,32].

In order to observe the initial stage of hydrogen intercalation, we developed an experimental setup for annealing in a high-pressure hydrogen gas atmosphere and for raising or lowering the temperature quickly. Figure 1(a) schematically illustrates the setup. We used an SUS316L stainless-steel tube with an inner diameter of 6 mm as a sample chamber. The following procedures were conducted to introduce hydrogen gas to the sample chamber before annealing. First, we evacuated the chamber with the buffer layer sample inside to $\sim 5 \times 10^{-5}$ Pa by a turbo-molecular pump. Next, H_2 gas with the purity of 99.9999%, further purified through an Applied Energy Systems 125C-S04-H2/Ar-FP ultrahigh-purity gas filter, was introduced to a pressure of 5.5 atm. To maintain the inner pressure constant during the annealing, a KOFLOC model6800B back-pressure valve was used. The sample chamber, filled with hydrogen gas, was then inserted into a tube furnace, which was preliminarily heated to 600 °C and was kept at this temperature. The sample chamber was held in the furnace for 60–2400 s, and then it was ejected from the furnace and cooled to room temperature. In this way, we annealed the buffer layer sample under a high-pressure hydrogen gas atmosphere and achieved an annealing time that was controlled in seconds to systematically observe the initial stage of hydrogen intercalation.

The growth of the buffer layer and the occurrence of hydrogen intercalation were confirmed by Raman spectroscopy at an ambient condition using a laser with an excitation wavelength of 532 nm and with a laser spot size of about 1 μm^2. The Raman signal of the initial SiC substrate was subtracted from all original Raman spectra to distinguish between the buffer layer and graphene components. Raman mapping was also performed over an area of 15×15 μm^2 with a scanning step size of 0.3 μm. Atomic force microscopy (AFM) measurements were carried out in the dynamic force mode to obtain topography and phase images of the sample surfaces. The atomic-scale structure of the interface was investigated by high-resolution transmission electron microscope (HRTEM) observations using a JEM-2010F microscope at an acceleration voltage of 200 kV. The thin specimens for TEM observations were prepared by the conventional Ar-ion thinning method. Details of this procedure are described in our previous papers [5,9,10,33,34].

III. RESULTS AND DISCUSSION

The experimental results are shown in the following three subsections. In the first subsection, the effect of the high-pressure hydrogen gas atmosphere on the decoupling of the buffer layer from the SiC substrate is examined. Based on the results of the first subsection, the initial stage of hydrogen intercalation is investigated in the second subsection. In the third subsection, hydrogen migration at the interface is discussed.

A. Effects of high-pressure hydrogen atmosphere

We first investigated the effect of high-pressure on the hydrogen intercalation. Figure 1(b) shows the Raman spectra for the samples annealed at 600 °C for 40 min under different hydrogen gas pressures. The spectra are normalized by the *G*-band intensity. In general, several broad peaks can be seen around 1200–1600 cm^{-1} in the buffer layer [35]. In monolayer graphene, *G* and 2*D* bands appear at ~1580 and ~ 2680 cm^{-1}, respectively, while a *D* band is observed at ~ 1350 cm^{-1} in the presence of defects in the graphene lattice [36]. In the sample annealed under the pressure of 1 atm, the spectrum can be explained by a mixture of the buffer layer and graphene peaks. In other words, hydrogen intercalation was not completed in this sample. However, the buffer layer feature decreased markedly with increasing pressure, and at 5.5 atm only graphene-derived peaks are found. At 5.5 atm, the position and the full width at half maximum (FWHM) of the 2*D* band were about 2677 and 28 cm^{-1}, respectively, suggesting the formation of QFMLG [16]. Moreover, the *D*-band intensity tends to decrease with increasing pressure. These results suggest that increasing the hydrogen gas pressure enhances the conversion of the buffer layer to QFMLG. Sun *et al.* reported a similar tendency at relatively low hydrogen partial pressures (10^{-2}–10^2 mbar) [25]. The tendency of the *D*-band intensity to decrease with increasing pressure is similar to the effect of increasing the hydrogen intercalation

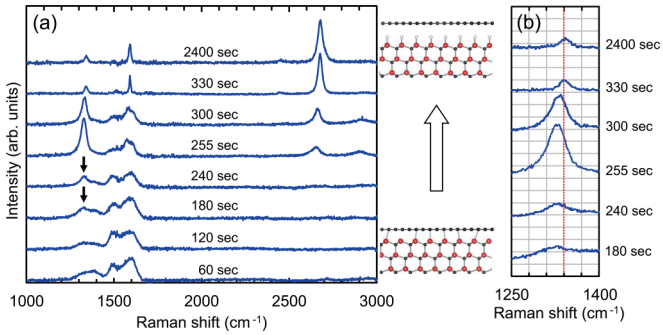

FIG. 2. (a) Raman spectra of the samples annealed for different durations at 600 °C in hydrogen gas at 5.5 atm. (b) Spectra around 1250–1400 cm^{-1} extracted for visibility.

temperature seen in some previous studies [21,23]. We also examined the temperature dependence of hydrogen intercalation. At an annealing temperature of 400 °C, there was no spectral change in the peak of the buffer layer, but as the temperature was increased above 500 °C, the characteristic bands of graphene gradually appeared (see Fig. S1 of Supplemental Material [37]). Generally, it is known that hydrogen intercalation phenomenon sufficiently proceeds at more than 600 °C [23,24]. These results indicate that we can lower the temperature of hydrogen intercalation by raising the hydrogen gas pressure. It is also known that at higher temperatures above around 800 °C, deintercalation starts to take place [11]. Thus, lower temperature and higher pressure would be desirable for effective intercalation treatment.

Note that a detailed focus on the temperature dependence would provide the activation energy of the whole process. It is an important attempt to relate the four variables (temperature, pressure, time, and activation energy) and discuss whether the activation energy should be overcome within the experimental condition. However, hydrogen intercalation consists of multiple elementary processes such as hydrogen impingement, hydrogen penetration into the buffer layer/SiC interface, decoupling of the Si–C bonds, and termination of the Si dangling bonds, and then it is difficult to identify which specific process is the rate-limiting step that determines the activation energy of the whole process. On the other hand, we believe that some quantitative arguments for any of the variables are useful. The unique point of our study is the achievement of the control of annealing time in seconds. Thus, in this study, we will mainly focus on the time evolution at fixed temperature and pressure of 600 °C and 5.5 atm, respectively, attempting to capture the progression of hydrogen intercalation.

B. Initial stage of hydrogen intercalation

We then focused on the initial stage of hydrogen intercalation by varying the annealing time. Hereafter, the annealing temperature and pressure were fixed at the values of 600 °C and 5.5 atm, respectively. Figure 2(a) shows the Raman spectra of the samples obtained at different annealing times. In the samples annealed for 60, 120, 180, and 240 s, typical buffer layer spectra are observed around 1200–1600 cm^{-1}. When we carefully inspect the 180- and 240-s samples, a slight increase in the *D*-band intensity, indicated by the arrows, can be seen. In the 255-s sample, a distinct 2*D* band appears, in addition to a further increase in *D*-band intensity. The 300-s sample shows a slight decrease in *D*-band intensity and an increase in 2*D*-band intensity. The $D + D'$ peaks are also observed in the spectra of the 255- and 300-s samples, suggesting a high defect density. At 330 s, sharper graphene peaks can be seen, while the buffer layer feature almost disappears. In addition, the *D*-band intensity is significantly reduced. At 2400 s, very little change was observed compared to the 330-s result. To sum up these results, the buffer layer remained unchanged until about 200 s after the start of annealing at 600 °C, and hydrogen intercalation occurred rapidly during the next 100 s. After 330 s, the QFMLG showed no significant change. A striking feature of the intercalation process is that a large number of defects were introduced in the initial stage, but they almost disappeared coincidently with the completion of intercalation. It is also important to note that the *D*-band positions at 240–300 s are slightly different from those after 330 s, as shown in Fig. 2(b), suggesting the presence of different types of defects.

Here, the possible types of defects are carbon deficiencies and graphene edges. However, it is unlikely that the restoration of a large number of carbon deficiencies would occur at 600°C. Therefore, the origin of the *D* band which became weaker after 300 s can be ascribed to the edge of the graphene, specifically the boundary between QFMLG and the un-decoupled buffer layer. In other words, the fact that the *D*-band intensity once increased suggests that the graphene/buffer layer boundaries are often present in the initial stage of hydrogen intercalation. The difference in the *D*-band positions shown in Fig. 2(b) implies that the defects in the graphene edge present in the initial stage and those remaining in the QFMLG after the completion of intercalation are intrinsically different. One candidate for the origin of the *D* band after complete intercalation is the point defect induced by hydrogen deficiency [20]. Further investigation of this *D*-band difference is needed in the future.

We then conducted AFM and HRTEM observations to investigate the relationship between the spectral changes presented above and the microscopic structure at the surface and interface. Figure 3 shows the AFM and HRTEM images of the samples obtained from the buffer layer, 300-, and 330-s samples. In HRTEM observations, the electron incidence was parallel to the $[11\bar{2}0]_{SiC}$ direction and the interlayer distances were measured on the basis of the lattice constant of 4H-SiC ($c = 1.008$ nm). For the buffer layer sample, one can see the step-terrace structure of the SiC substrate surface in the AFM topography image shown in Fig. 3(a) and dark and bright contrast in the phase image in Fig. 3(b). Since the feature of the buffer layer was dominant in the Raman spectrum before hydrogen intercalation as shown in Fig. 2(a), the darker areas in Fig. 3(b), which cover most of the sample surface, correspond to the buffer layer, while the brighter areas near the step edges correspond to partially grown monolayer graphene. This observation is consistent with the graphene nucleation at the step edges in the SiC thermal decomposition method, as previously reported [33]. It should be noted here that the sample annealed for 180 s also exhibited similar surface topography. In the HRTEM image of this sample in Fig. 3(c), layered contrasts were observed. Although most of the area in this sample was covered by a single layer, here we show an image where

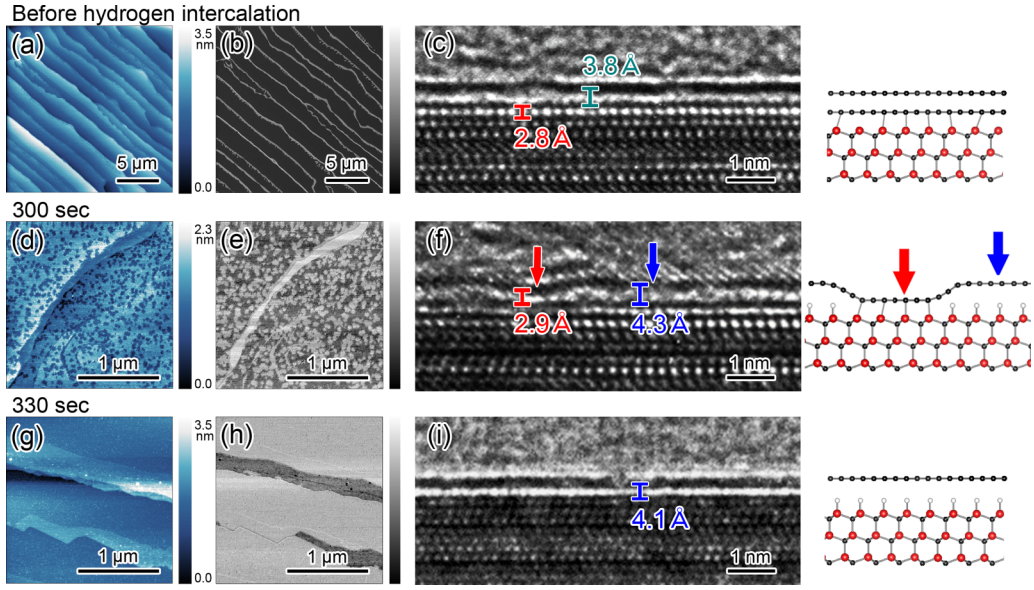

FIG. 3. AFM topography bluescale and phase grayscale images and HRTEM images of (a)–(c) the buffer layer sample before hydrogen intercalation, (d)–(f) the sample annealed at 600 °C for 300 s, and (g)–(i) the sample annealed at 600°C for 330 s. A schematic representation of the cross-sectional structure is shown on the right side of each HRTEM image.

two layers were observed as dark-line contrast. The interlayer distance between the first and second layers was found to be 3.8 Å, while that of the second and the underlying layer was 2.8 Å. These values are in good agreement with the distances between graphene and the buffer layer (3.5 Å) and between the buffer layer and the top SiC surface (2.9 Å) in previous studies, respectively [5]. Therefore, this HRTEM image indicates the formation of the buffer layer and a monolayer of graphene on top of it, as schematically illustrated on the right side of Fig. 3(c). As indicated from the Raman spectrum at 300 s, the buffer layer and QFMLG coexisted, while after 330 s the buffer layer disappeared and only QFMLG was present on the SiC substrate. The AFM images of the 300-s sample presented in Figs. 3(d) and 3(e) indicate that the surface topography has microscopic bumps with a height of less than 1 nm in the terraces, and they have the corresponding phase difference. Here, hydrogen intercalation increases the height of the graphene sheet from the SiC substrate due to the inserted hydrogen atoms at the interface [17,19,22,38]. Thus, the convex area is considered to be the region where hydrogen intercalation occurred. Figure 3(f) shows an HRTEM image of the sample which showed the local height difference. Interestingly, as indicated by the red and blue arrows, the line contrast shows different distances from the top SiC surface layer, which are 2.9 and 4.3 Å, respectively. Each of these values is in good agreement with the distances of the buffer layer and QFMLG from the top SiC surface layer determined in previous studies using x-ray diffraction experiments [17,38]. Therefore, the red arrow indicates the region where the buffer layer remains locally un-decoupled, while the rest of the surface was hydrogen intercalated, as schematically illustrated in the right side of Fig. 3(f). In other words, there are many boundaries between the buffer layer and QFMLG on the terrace, which is consistent with the high *D*-band intensity in the Raman spectrum. Meanwhile, at 330 s, the terraces were smooth in the topography image in Fig. 3(g) and there was no phase difference within the terraces in the phase image shown in Fig. 3(h). These suggest that QFMLG uniformly covered the sample surface. For the HRTEM image shown in Fig. 3(i), a dark-line contrast on the SiC substrate surface can be seen, suggesting the presence of the uniform QFMLG. The distance of the graphene layer from the SiC top surface was 4.1 Å over the entire observed area.

From these experimental results, it is understood that hydrogen intercalation occurs locally and simultaneously throughout the terraces in the initial stage, and that graphenization proceeds over the entire surface of the terraces by expanding the intercalated area. We discuss the microscopic mechanism of this initial stage more in detail. Figure 4 shows the time evolution of QFMLG coverage estimated from the

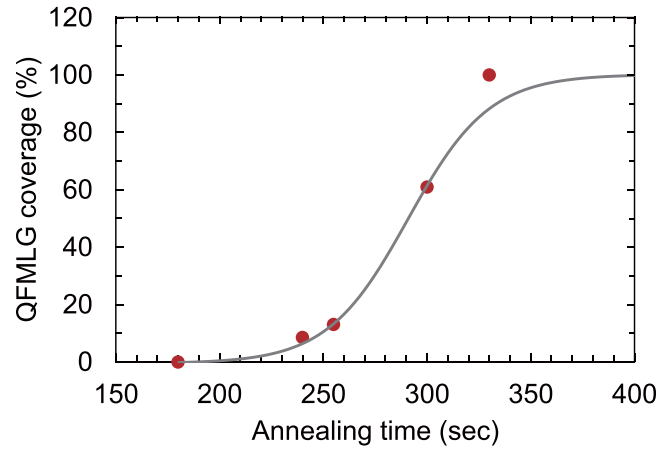

FIG. 4. Time evolution of the QFMLG coverage during hydrogen intercalation at 600 °C in a pressure of 5.5 atm. Each dot represents the QFMLG coverage determined from the AFM phase images at that annealing time. The solid line is the theoretical curve based on Ref. [39].

AFM images. Again, the annealing temperature and pressure were 600 °C and 5.5 atm, respectively. The QFMLG coverage at each annealing time was defined from the area ratio of the two types of contrasts in the AFM phase image and plotted in dots. As mentioned previously, only buffer layer is present on the SiC surface at 180 s and only QFMLG at 330 s. In the transition between these, QFMLG coverage increases gradually in the very early stage, but then increases drastically to complete decoupling. In other words, the conversion of the buffer layer to QFMLG does not proceed linearly. Here, Suemitsu *et al.* reported an interesting study on the kinetics of the initial stage of thermal oxidation of Si surface [39]. They derived a rate equation for the oxidation based on the dual-oxide species model and showed that it can describe the time evolution of the coverage of Si surface oxide. The progression of oxidation on the Si (100) surface at 640 °C was explained by the two-dimensional (2D)-island growth mode, and the time evolution of the coverage was well fitted by a sigmoidlike function. This sigmoidal time evolution reflects the nucleation-growth-coalescence nature of the island growth. The solid line in Fig. 4 is the theoretical curve based on their rate equation. The time evolution of QFMLG coverage by hydrogen intercalation was also found to be well fitted by this sigmoidlike function. Therefore, it is understood that hydrogen intercalation proceeds through the expansion and coalescence of locally formed 2D islands of QFMLG. The expansion of the QFMLG island is considered to proceed by in-plane migration of interfacial hydrogen atoms forming Si–H bonds. This hydrogen migration will be discussed in the next subsection. Here, at 330 s, graphenization was completed earlier than the theoretical curve. According to Ref. [39], the behavior of the final stage of this theoretical curve is related to the randomness of the distribution of 2D islands nucleated in the very early stage. If the homogeneity of the distribution is high, the increase of the coverage in the final stage becomes steeper. Therefore, the rapid completion of termination around 330 s can be attributed to the relatively homogeneous occurrence of QFMLG islands at the very early stage. Note that the number of data points that can be obtained in our present experiment is not large. In order to gain more detailed insights, experiments that can continuously follow the evolution of the coverage (e.g., *in situ* radiation microscopy [40]) are needed, which is our future task.

In addition, the fact that hydrogen intercalation occurred throughout the terraces suggests that the hydrogen did not enter the interface predominantly from the surface step, but penetrated the buffer layer on the terrace to reach the interface. However, in some theoretical studies based on first-principles calculations [28,29,41], the penetration of hydrogen through the buffer layer is a rare event due to a high-energy barrier. Here, all of these studies pointed out that the presence of defects such as vacancies facilitates the penetration. Therefore, intrinsic defects in the buffer layer [42] may have helped the hydrogen penetration, resulting in the local and simultaneous intercalation throughout the terraces.

C. Hydrogen migration at the interface

1. *Hydrogen migration across the step with subnanometer height*

In the previous subsection, we showed that hydrogen intercalation completed over the entire surface at 330 s. We then aimed to observe the surface morphology just before the completion. Figure 5 shows the AFM images of the sample treated for 315 s at 600 °C and a hydrogen gas pressure of 5.5 atm. As indicated by the blue and red arrows in the topography image in Fig. 5(a), smooth terraces and terraces with a height difference on the surface, respectively, were observed simultaneously. In the phase image in Fig. 5(b), almost no phase difference was identified on the smooth terraces, while the larger phase difference can be seen on the terraces with the height difference. This indicates that terraces where hydrogen intercalation was almost completed and terraces where it was not completed coexist as illustrated in Fig. 5(c). In other words, hydrogen intercalation completed terrace by terrace. As mentioned in the previous subsection, hydrogen intercalation is considered to proceed by in-plane migration of interfacial hydrogen atoms forming Si–H bonds. Thus, this result suggests that entered hydrogen at the interface migrates easily in a direction parallel to the step, but has difficulty hopping across the step whose height was about 2 nm.

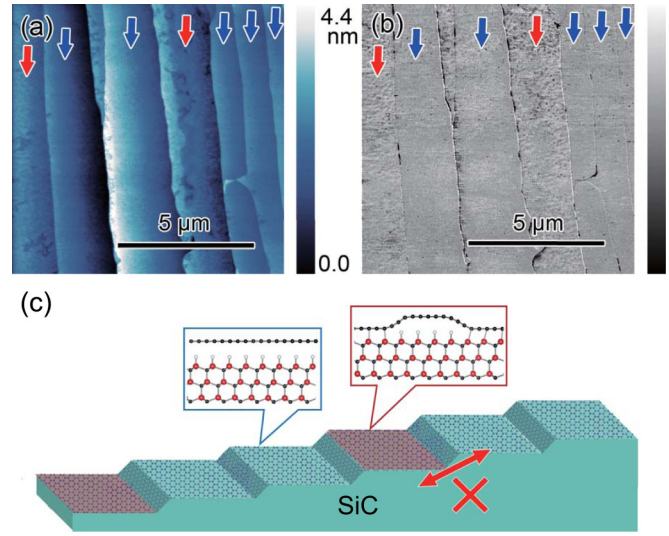

FIG. 5. AFM topography (a) and phase (b) images of the sample annealed for 315 s, with a schematic illustration of these AFM images (c).

2. *Hydrogen migration across the step of one SiC bilayer*

In addition to the above result, we further discuss the hydrogen migration across the lower atomic step with a height of 0.25 nm, which corresponds to one Si-C bilayer height. Figures 6(a) and 6(b) show Raman mapping images acquired in a 15×15-μm^2 area of a sample treated for 2400 s at a temperature of 600 °C and a hydrogen gas pressure of 5.5 atm. The mapping image by FWHM of the 2*D* band in Fig. 6(a) shows a contrast that clearly reflects the step-terrace structure of the SiC surface. The FWHM at the terraces and the step edges were 25–30 and 30–45 cm^{-1}, respectively. In general, the FWHM of the 2*D* band is about 30 cm^{-1} for monolayer graphene, and tends to increase with the number of layers [36]. Thus, monolayer graphene covers the terraces, while bilayer graphene partly exists near the step edges. This

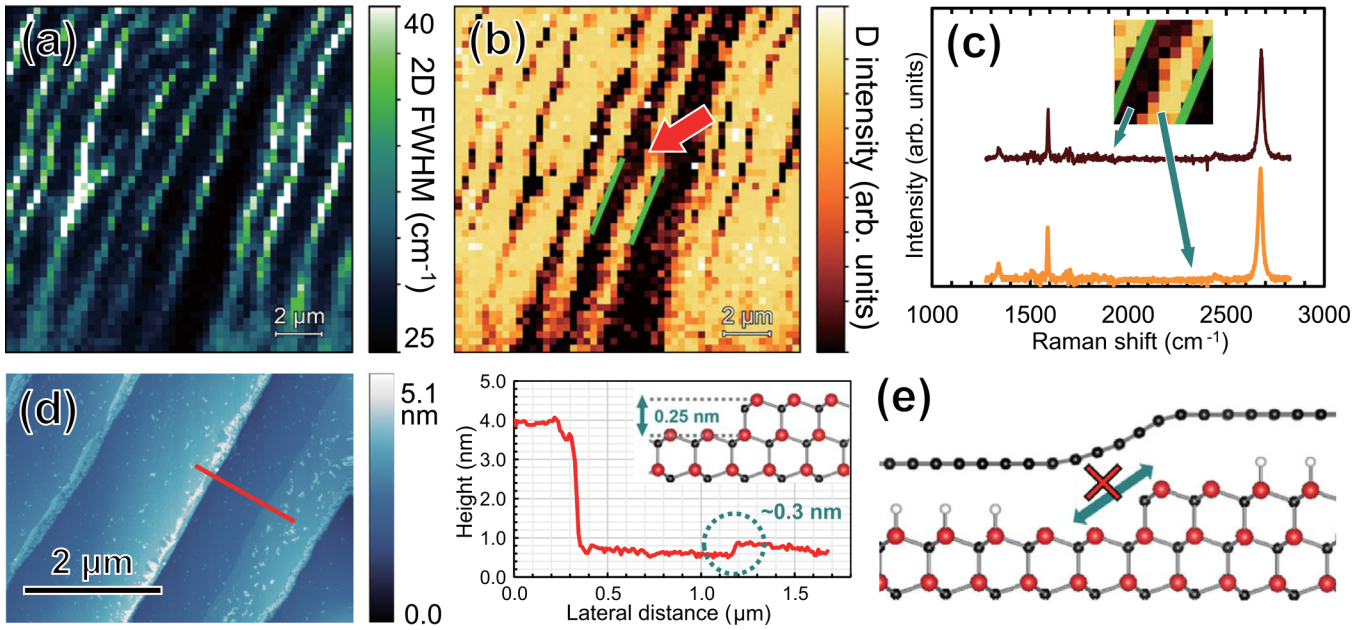

FIG. 6. Raman mapping images of (a) FWHM of the 2*D* band and (b) the *D*-band intensity of the sample annealed for 2400 s. (c) Raman spectra extracted from the left and right sides of the boundary indicated by the arrow in (b). (d) The AFM topography image of this sample with the height profile acquired on the red line. (e) Schematic representation of hydrogen diffusion across the step of one SiC bilayer, indicating that it is difficult for hydrogen at the interface to diffuse beyond this atomic step.

means that the buffer layer and partly formed monolayer graphene around the step edges were converted into QFMLG and quasi-freestanding bilayer graphene by hydrogen intercalation, respectively. The mapping image of *D*-band intensity shown in Fig. 6(b) shows a similar step-terrace structure to that of Fig. 6(a). The green solid lines in Fig. 6(b) indicate the step edges identified in Fig. 6(a) where the FWHM of the 2*D* band is broader. In other words, the region sandwiched by these two solid lines corresponds to a terrace. Here, as indicated by an arrow in Fig. 6(b), there is a boundary in the distribution of the *D*-band intensity within a terrace. Figure 6(c) shows the spectra acquired on the left and right sides of the boundary indicated by the arrow. The general shapes of the two spectra are similar, with a slight difference in the *D*-band intensity. This indicates that the QFMLG covers both sides of the arrow. The difference in the *D*-band intensity is caused by the number of defects in graphene, such as point defects induced by hydrogen deficiency. This distribution of defects reminds us that hydrogen at the interface migrated easily in a direction parallel to the step but had difficulty in hopping over the step, which was discussed in Fig. 5.

In order to clarify the details of this distribution of the defect density within the same terrace, a more precise AFM observation on the surface morphology was performed. Figure 6(d) shows the AFM topography image of this sample, together with the height profile acquired along the red line. As shown by the dotted circle, a height difference of about 0.3 nm was observed on a terrace. This feature was also observed in the buffer layer sample before hydrogen intercalation (see Fig. S2 of Supplemental Material [37]). Therefore, it can be inferred that this height difference in the terrace is not due to the difference in the number of graphene layers, but comes from the atomic step of one Si-C bilayer of the 4H-SiC substrate with a height of 0.25 nm, as shown in the inset. In other words, there are regions with different defect density in graphene on the upper and lower sides of the one Si-C bilayer step. This suggests that hydrogen at the interface is hard to migrate beyond the step of one SiC bilayer, as schematically illustrated in Fig. 6(e).

As we discussed in Sec. III B, hydrogen intercalation is suggested to initiate locally and simultaneously throughout the terraces. Here, if the probability of local intercalation occurrence is perfectly the same on all terraces, the hydrogen migration across the steps would not matter. In practice, however, as shown in Fig. 6, QFMLG was slightly inhomogeneous across the step, even after annealing for 2400 s. We consider that this is due to the Ehrlich-Schwoebel (ES) barrier. In fact, Wundrack *et al.* experimentally showed that the ES barrier on the SiC steps retards the propagation of Ga atoms at the graphene/SiC interface in Ga intercalation [43]. Our results suggest that even the migration of the smallest H atoms can be hindered by the ES barrier on the SiC steps, giving rise to QFMLG with slightly different quality above and below the steps. Therefore, in electronic application of QFMLG, it may be necessary to selectively fabricate a device onto terraces avoiding steps.

IV. CONCLUSIONS

We have investigated the microscopic mechanism of hydrogen intercalation at the buffer-layer/SiC interface. Hydrogen intercalation was suggested to initiate locally and simultaneously on the terrace, not at the step edge. Inserted hydrogen then migrate in the interface, resulting in full graphenization over the SiC surface. These experimental

observations suggest that hydrogen can penetrate the buffer layer, which might be due to its intrinsic defects. In addition, the steps on the SiC surface with a height even as low as 0.25 nm acted as the hydrogen migration barrier. These findings provide significant insights into the fundamental mechanism of hydrogen intercalation, for which there has been no unified view despite many investigations, and may contribute to the development of graphene electronics.

ACKNOWLEDGMENTS

This work was supported by JSPS KAKENHI Grants No. JP18H01889, No. JP20H05287, and No. JP21J23576. This work was partly carried out at the Joint Research Center for Environmentally Conscious Technologies in Materials Science (Project No. 31001, 02009, and 02105) at ZAIKEN, Waseda University. We also thank Dr. Tomo-o Terasawa for valuable discussions.

[1] C. Berger, Z. Song, T. Li, X. Li, A. Y. Ogbazghi, R. Feng, Z. Dai, N. Alexei, M. E. H. Conrad, P. N. First, and W. A. De Heer, J. Phys. Chem. B **108**, 19912 (2004).

[2] K. V. Emtsev, A. Bostwick, K. Horn, J. Jobst, G. L. Kellogg, L. Ley, J. L. McChesney, T. Ohta, S. A. Reshanov, J. Röhrl, E. Rotenberg, A. K. Schmid, D. Waldmann, H. B. Weber, and T. Seyller, Nat. Mater. **8**, 203 (2009).

[3] Y. M. Lin, C. Dimitrakopoulos, K. A. Jenkins, D. B. Farmer, H. Y. Chiu, A. Grill, and P. Avouris, Science **327**, 662 (2010).

[4] P. Avouris and F. Xia, MRS Bull. **37**, 1225 (2012).

[5] W. Norimatsu and M. Kusunoki, Chem. Phys. Lett. **468**, 52 (2009).

[6] C. Riedl, U. Starke, J. Bernhardt, M. Franke, and K. Heinz, Phys. Rev. B **76**, 245406 (2007).

[7] J. Jobst, D. Waldmann, F. Speck, R. Hirner, D. K. Maude, T. Seyller, and H. B. Weber, Phys. Rev. B **81**, 195434 (2010).

[8] A. Bostwick, T. Ohta, T. Seyller, K. Horn, and E. Rotenberg, Nat. Phys. **3**, 36 (2007).

[9] Y. Masuda, W. Norimatsu, and M. Kusunoki, Phys. Rev. B **91**, 075421 (2015).

[10] J. Bao, W. Norimatsu, H. Iwata, K. Matsuda, T. Ito, and M. Kusunoki, Phys. Rev. Lett. **117**, 205501 (2016).

[11] C. Riedl, C. Coletti, T. Iwasaki, A. A. Zakharov, and U. Starke, Phys. Rev. Lett. **103**, 246804 (2009).

[12] C. Virojanadara, S. Watcharinyanon, A. A. Zakharov, and L. I. Johansson, Phys. Rev. B **82**, 205402 (2010).

[13] S. Oida, F. R. McFeely, J. B. Hannon, R. M. Tromp, M. Copel, Z. Chen, Y. Sun, D. B. Farmer, and J. Yurkas, Phys. Rev. B **82**, 041411(R) (2010).

[14] Z. Y. Al Balushi, K. Wang, R. K. Ghosh, R. A. Vilá, S. M. Eichfeld, J. D. Caldwell, X. Qin, Y. C. Lin, P. A. Desario, G. Stone, S. Subramanian, D. F. Paul, R. M. Wallace, S. Datta, J. M. Redwing, and J. A. Robinson, Nat. Mater. **15**, 1166 (2016).

[15] I. Gierz, T. Suzuki, R. T. Weitz, D. S. Lee, B. Krauss, C. Riedl, U. Starke, H. Höchst, J. H. Smet, C. R. Ast, and K. Kern, Phys. Rev. B **81**, 235408 (2010).

[16] F. Speck, J. Jobst, F. Fromm, M. Ostler, D. Waldmann, M. Hundhausen, H. B. Weber, and T. Seyller, Appl. Phys. Lett. **99**, 2009 (2011).

[17] J. Sforzini, L. Nemec, T. Denig, B. Stadtmüller, T.-L. Lee, C. Kumpf, S. Soubatch, U. Starke, P. Rinke, V. Blum, F. C. Bocquet, and F. S. Tautz, Phys. Rev. Lett. **114**, 106804 (2015).

[18] S. Forti, K. V. Emtsev, C. Coletti, A. A. Zakharov, C. Riedl, and U. Starke, Phys. Rev. B **84**, 125449 (2011).

[19] K. Yamasue, H. Fukidome, K. Funakubo, M. Suemitsu, and Y. Cho, Phys. Rev. Lett. **114**, 226103 (2015).

[20] Y. Murata, T. Cavallucci, V. Tozzini, N. Pavliček, L. Gross, G. Meyer, M. Takamura, H. Hibino, F. Beltram, and S. Heun, Nano Res. **11**, 864 (2018).

[21] J. Kunc, M. Rejhon, and P. Hlídek, AIP Adv. **8**, 045015 (2018).

[22] S. Watcharinyanon, C. Virojanadara, J. R. Osiecki, A. A. Zakharov, R. Yakimova, R. I. G. Uhrberg, and L. I. Johansson, Surf. Sci. **605**, 1662 (2011).

[23] J. A. Robinson, M. Hollander, M. Labella, K. A. Trumbull, R. Cavalero, and D. W. Snyder, Nano Lett. **11**, 3875 (2011).

[24] S. Tanabe, M. Takamura, Y. Harada, H. Kageshima, and H. Hibino, Jpn. J. Appl. Phys. **53**, 04EN01 (2014).

[25] C. Sun, W. Cai, R. Hong, J. Wu, X. Chen, J. Cai, F. Zhang, and Z. Wu, J. Phys. Chem. Solids **137**, 109224 (2020).

[26] Y. Murata, M. Takamura, H. Kageshima, and H. Hibino, Phys. Rev. B **87**, 165408 (2013).

[27] T. A. de Jong, E. E. Krasovskii, C. Ott, R. M. Tromp, S. J. van der Molen, and J. Jobst, Phys. Rev. Mater. **2**, 104005 (2018).

[28] A. Markevich, R. Jones, S. Öberg, M. J. Rayson, J. P. Goss, and P. R. Briddon, Phys. Rev. B **86**, 045453 (2012).

[29] B. Lee, S. Han, and Y.-S. Kim, Phys. Rev. B **81**, 075432 (2010).

[30] C. Virojanadara, M. Syväjarvi, R. Yakimova, L. I. Johansson, A. A. Zakharov, and T. Balasubramanian, Phys. Rev. B **78**, 245403 (2008).

[31] T. Sumi, K. Nagai, J. Bao, T. Terasawa, W. Norimatsu, M. Kusunoki, and Y. Wakabayashi, Appl. Phys. Lett. **117**, 143102 (2020).

[32] Y. Saito, K. Tokiwa, T. Kondo, J. Bao, T. Terasawa, W. Norimatsu, and M. Kusunoki, AIP Adv. **9**, 065314 (2019).

[33] W. Norimatsu and M. Kusunoki, Phys. E (Amsterdam, Neth.) **42**, 691 (2010).

[34] W. Norimatsu, K. Matsuda, T. O. Terasawa, N. Takata, A. Masumori, K. Ito, K. Oda, T. Ito, A. Endo, R. Funahashi, and M. Kusunoki, Nanotechnology **31**, 145711 (2020).

[35] F. Fromm, M. H. Oliveira Jr, A. Molina-Sánchez, M. Hundhausen, J. M. J. Lopes, H. Riechert, L. Wirtz, and T. Seyller, New J. Phys. **15**, 043031 (2013).

[36] A. C. Ferrari, J. C. Meyer, V. Scardaci, C. Casiraghi, M. Lazzeri, F. Mauri, S. Piscanec, D. Jiang, K. S. Novoselov, S. Roth, and A. K. Geim, Phys. Rev. Lett. **97**, 187401 (2006).

[37] See Supplemental Material at http://link.aps.org/supplemental/10.1103/PhysRevB.105.235442 for Raman results at different annealing temperatures and AFM images of the sample before hydrogen intercalation.

[38] J. D. Emery, V. H. Wheeler, J. E. Johns, M. E. McBriarty, B. Detlefs, M. C. Hersam, D. Kurt Gaskill, and M. J. Bedzyk, Appl. Phys. Lett. **105**, 161602 (2014).

[39] M. Suemitsu, Y. Enta, Y. Miyanishi, and N. Miyamoto, Phys. Rev. Lett. **82**, 2334 (1999).
[40] T. Terasawa and K. Saiki, Nat. Commun. **6**, 6834 (2015).
[41] I. Deretzis and A. La Magna, Nanoscale **5**, 671 (2013).
[42] Y. Qi, S. H. Rhim, G. F. Sun, M. Weinert, and L. Li, Phys. Rev. Lett. **105**, 085502 (2010).
[43] S. Wundrack, D. Momeni, W. Dempwolf, N. Schmidt, K. Pierz, L. Michaliszyn, H. Spende, A. Schmidt, H. W. Schumacher, R. Stosch, and A. Bakin, Phys. Rev. Mater. **5**, 024006 (2021).